DOI 10.1021/la504906q

Langmuir

Article

pubs.acs.org/Langmuir

Size and Aspect Ratio Control of Pd_2Sn Nanorods and Their Water Denitration Properties

ZhiShan Luo,[†] Maria Ibáñez,[†] Ana M. Antolín,[‡] Aziz Genç,[§] Alexey Shavel,[†] Sandra Contreras,[‡] Francesc Medina,[‡] Jordi Arbiol,[§,∥] and Andreu Cabot*[,†,∥]

[†]Catalonia Institute for Energy Research (IREC), 08930 Sant Adrià del Besòs, Barcelona, Spain

[‡]Departament d'Enginyeria Química, Universitat Rovira i Virgili, Campus Sescelades, 43007 Tarragona, Tarragona, Spain

[§]Institut de Ciència de Materials de Barcelona (ICMAB), Consejo Superior de Investigaciones Científicas (CSIC), Campus de la Universitat Autònoma de Barcelona (UAB), 08193 Bellaterra, Barcelona, Spain

[∥]Institució Catalana de Recerca i Estudis Avançats (ICREA), 08010 Barcelona, Barcelona, Spain

Supporting Information

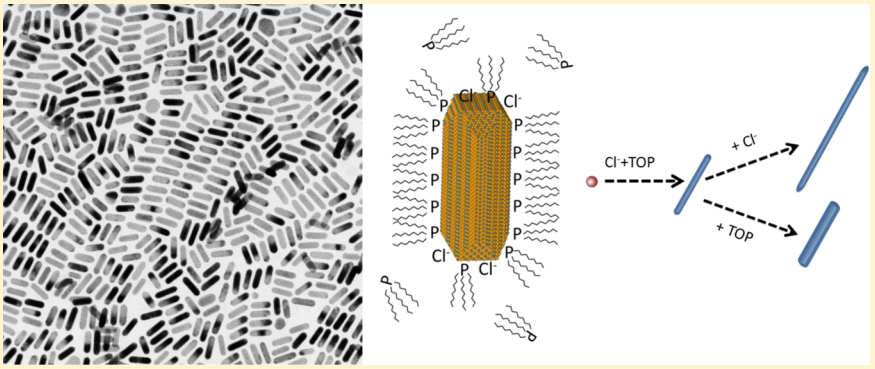

ABSTRACT: Monodisperse Pd_2Sn nanorods with tuned size and aspect ratio were prepared by co-reduction of metal salts in the presence of trioctylphosphine, amine, and chloride ions. Asymmetric Pd_2Sn nanostructures were achieved by the selective desorption of a surfactant mediated by chlorine ions. A preliminary evaluation of the geometry influence on catalytic properties evidenced Pd_2Sn nanorods to have improved catalytic performance. In view of these results, Pd_2Sn nanorods were also evaluated for water denitration.

INTRODUCTION

The development of alternative Pt-free catalysts with comparable or improved activities, selectivities, and stabilities is critical to reduce the cost of catalytic materials and processes. In this direction, bimetallic catalysts, including abundant elements, are one first step toward cost reduction.[1−3] In particular, Pd-based bimetallic particles with tuned chemical composition, electronic states, and synergy between the two metals have allowed for not only the reduction of material costs but also the improvement of performance and stability with respect to Pt-based and pure Pd catalysts.[4−6] As an example, Pd and Pd-based bimetallic catalysts are particularly suitable for hydrogenation and dehydrogenation reactions, carbon−carbon bond-forming reactions, such as Heck or Suzuki, and electrooxidation of primary alcohols.[7−11] Pd alloys with metals that bind strongly to oxygen also provide greater resistance to CO, C, and S poisoning.[12−17]

Besides composition, the shape of catalytic nanoparticles (NPs), which dictates surface facets and active reaction sites, is the other key parameter determining a catalyst performance.[18−20] However, because of the limitations of conventional impregnation methods to control NP geometry, this parameter is generally neglected during catalyst optimization. Colloidal synthesis methods allow for adjusting catalytic NP properties beyond conventional impregnation methods, offering the opportunity to design and engineer well-controlled model systems. In this direction, the development of synthetic routes to produce Pd-based bimetallic NPs with tuned size and shape has attracted significant effort in the past decade.[5,12−17,21] Among the various bimetallic NPs, Pd−Sn is a particularly interesting candidate for the ethanol oxidation reaction[22,23] and water denitration.[24,25] However, despite its interest, the synthesis of Pd−Sn NPs with controlled morphology still remains a major challenge.

Herein, we describe a synthetic route to produce highly monodisperse Pd_2Sn NPs with tuned size and morphology. Besides, we present here results from the functional characterization of the new materials produced. We preliminary tested

Received: December 18, 2014
Revised: March 7, 2015

DOI: 10.1021/la504906q
Langmuir XXXX, XXX, XXX−XXX

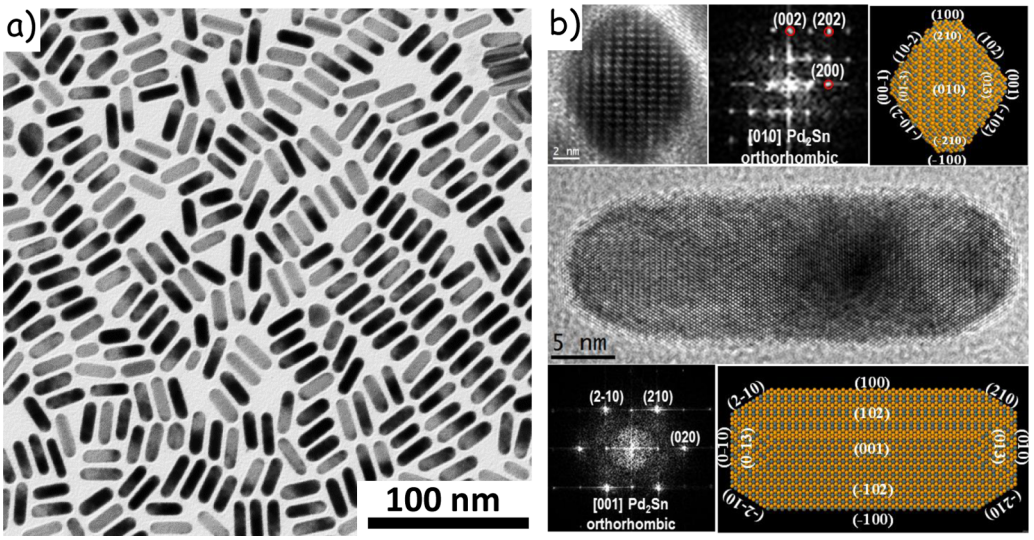

Figure 1. (a) TEM micrograph of 27 nm long and 9 nm wide Pd_2Sn NRs. (b) HRTEM micrographs, power spectra, and 3D atomic models of vertically and horizontally aligned Pd_2Sn NRs.

the catalytic properties of Pd_2Sn NPs using the reduction of *p*-nitrophenol by $NaBH_4$ as a model reaction.[26] Furthermore, the performance of TiO_2-supported Pd_2Sn nanorods (NRs) and nanospheres toward water denitration was also evaluated.

EXPERIMENTAL SECTION

Chemicals. Palladium(II) acetylacetonate [$Pd(acac)_2$, 99%], tin(II) acetylacetonate [$Sn(acac)_2$, 99.9%], oleylamine (OLA, >70%), 3-mercaptopropionic acid (MPA, ≥99%), oleic acid (OA, 90%), hexadecylamine (HDA, 90%), cyclohexanone ($C_6H_{10}O$, 99.8%), sodium hydroxide pellets (NaOH, ≥97%), and hydrochloric acid (37% in water) were purchased from Sigma-Aldrich. Tri-*n*-octylphosphine (TOP, 97%) was purchased from Strem. Hexane, chloroform, and ethanol were of analytical grade and obtained from various sources. Milli-Q water was supplied by the PURELAB flex from ELGA. All chemicals were used as received without further purification, except OLA, which was purified by distillation. All syntheses were carried out using standard airless techniques: a vacuum/dry argon gas Schlenk line was used for the syntheses, and an argon glovebox was used for storing and handling air and moisture-sensitive chemicals.

Preparation of Hexadecylammonium Chloride (HDA·HCl). HDA·HCl was prepared by the direct reaction of HDA with an aqueous solution of hydrochloric acid. A total of 20 mmol (4.83 g) of HDA was dissolved in 50 mL of acetone, and 30 mmol (2.96 g) of HCl (37% in water) was added dropwise to the solution. The white precipitate was kept stirring in solution overnight. The HDA·HCl precipitate was filtered out, thoroughly washed with Milli-Q water, and dried under vacuum.

Synthesis of Pd_2Sn Nanorods. In a typical synthesis, 5 mL of OLA, 0.2 mmol of HDA·HCl, and 0.075 mmol of $Pd(acac)_2$ were placed in a 25 mL four-neck flask and purged under argon flow for 30 min at 60 °C. Next, 0.25 mL of 0.1 M $Sn(acac)_2$ in TOP was injected. Upon injection, the solution color changed to dark yellow. The solution was heated to 200 °C at 12 °C/min and maintained at this temperature for 30 min. Afterward, the temperature was further increased to 300 °C at 2.5 °C/min and kept for an additional 30 min. During heating, the color changed gradually to black. Then, the solution was cooled to room temperature. While cooling, when the temperature reached approximately 70 °C, 1 mL of OA was added to improve nanoparticle (NP) solubility. Pd_2Sn NPs were separated from the reaction mixture by adding 20 mL of ethanol and centrifuging at 3000 rpm for 5 min. NPs were washed with chloroform as the solvent and ethanol as the non-solvent by multiple precipitation/redispersion steps.

Synthesis of Pd_2Sn Spherical NPs for Catalytic Performance Evaluation. Pd_2Sn spherical NPs were obtained following the same procedure used to produce Pd_2Sn NRs but without introducing HDA·HCl.

Synthesis of Pd Spherical NPs for Catalytic Performance Evaluation. Pd spherical NPs were prepared following the same procedure used to produce Pd_2Sn NRs but without introducing HDA·HCl and $Sn(acac)_2$ and setting the growth temperature to 200 °C and growth time to 30 min.

Ligand Exchange with Mercaptopropionic Acid (MPA). Pd_2Sn NPs dispersed in hexane (~50 mg in 5 mL) were mixed with 5 mL of MPA and 5 mL of cyclohexanone. The mixture was sonicated for 30 min. Subsequently, NPs were centrifuged, and the precipitate was further washed with 10 mL of cyclohexanone, chloroform, and ethanol, successively. Finally, NPs were dissolved in 2.25 mL of deionized water with 0.25 mL of 0.2 M NaOH solution.

***p*-Nitrophenol Reduction.** The kinetics of catalytic reduction of *p*-nitrophenol to *p*-aminophenol was monitored by the color change involved in the reaction. Aqueous solutions of *p*-nitrophenol (1.4 mM) and $NaBH_4$ (0.42 M) were freshly prepared as separate stock solutions. Deionized water (13.0 mL) was mixed with 1.5 mL of *p*-nitrophenol stock solution. Then, 5 mL of MPA-coated Pd_2Sn NR catalysts in water containing 0.1 mL of 0.2 M NaOH solution was added to the mixture with a final concentration of 0.05 mg/mL or 1.4×10^8 NRs/mL. After mixing, 19.5 mL of the reaction solution was quickly transferred to a quartz cuvette. Then, 0.5 mL of $NaBH_4$ stock solution was injected into the quartz cuvette, and the absorbance spectra were successively recorded with a 5 s period using an ultraviolet−visible (UV−vis) spectrometer until the pale brown solution became colorless. To properly compare each type of catalyst, we keep the same amount for all catalysts (0.05 mg/mL). A total of 5 mL of Pd (3.1 nm in size) and Pd_2Sn (4.9 nm in size) NP catalyst aqueous solution separately was used with a final concentration of 3.4×10^{11} and 6.8×10^{11} NPs/mL, respectively (see the Supporting Information).

Water Denitration. For the nitrate heterogeneous catalytic reduction reaction, 5% Pd_2Sn spherical NPs and NRs were supported on Aeroxide TiO_2 P25 powder form. A constant hydrogen flow (150 mL/min) was used as a reducing agent to transform nitrate into nitrogen gas as the desirable product.

Denitration experiments were performed in a 350 mL polytetrafluoroethylene (PTFE) batch reactor under standard operational conditions (atmospheric pressure and room temperature). Sodium nitrate ($NaNO_3$) was used as the nitrate source in ultrapure water. The amount of 0.2 g of catalyst was introduced in the 100 ppm nitrate (NO_3^-) solution and remained in suspension by continuously stirring

DOI: 10.1021/la504906q
Langmuir XXXX, XXX, XXX−XXX

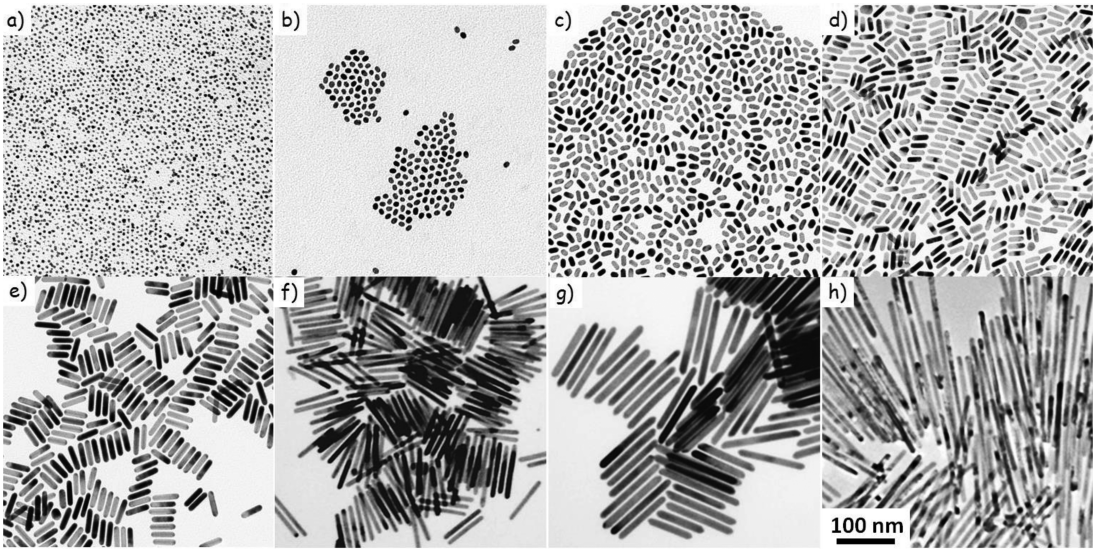

Figure 2. TEM micrographs of Pd_2Sn NPs with different aspect ratios (AR): (a) 4.3 ± 0.2 nm, AR = 1; (b) 9 ± 1 nm × 6.8 ± 0.6 nm, AR = 1.3; (c) 15 ± 1 nm × 7 ± 1 nm, AR = 2.1; (d) 24 ± 2 nm × 7 ± 1 nm, AR = 3.4; (e) 44 ± 4 nm × 10 ± 2 nm, AR = 4.4, (f) 98 ± 8 nm × 9 ± 1 nm, AR = 10.8; (g) 130 ± 10 nm × 24 ± 4 nm, AR = 5.4; and (h) 290 ± 20 nm × 12 ± 3 nm, AR = 24.2.

at 500 rpm. Samples were periodically withdrawn to analyze NO_3^- and reaction byproducts, such as nitrite (NO_2^-) and ammonia (NH_4^+) ions, which were quantified by photometry (PC MultiDirect Lovibond).

■ RESULTS AND DISCUSSION

Pd−Sn NPs were prepared by co-reducing $Pd(acac)_2$ and $Sn(acac)_2$ in the presence of amines, TOP, and chlorine ions. In a typical synthesis, 5 mL of OLA, 0.2 mmol of HDA·HCl, and 0.075 mmol of $Pd(acac)_2$ were placed in a 25 mL four-neck flask and purged under argon flow for 30 min. Next, 0.25 mL of a 0.1 M $Sn(acac)_2$ solution in TOP was injected, and the mixture was heated to 200 °C at 12 °C/min and maintained at this temperature for 30 min. Finally, the solution was heated to 300 °C at 2.5 °C/min, and NPs were allowed to grow for 30 min before cooling to room temperature. Finally, NPs were purified by multiple precipitation/redispersion steps.

Figure 1 displays representative transmission electron microscopy (TEM) and high-resolution transmission electron microscopy (HRTEM) micrographs of Pd−Sn NPs obtained by the procedure described above. Pd−Sn NPs were characterized by very narrow size distributions and rod-like geometry.

Power spectrum analysis revealed Pd−Sn NRs to have an orthorhombic Pd_2Sn phase (space group *Pnma*) with lattice parameters a = 0.5635 nm, b = 0.4283 nm, and c = 0.8091 nm. The NR growth direction was identified as [010]. HRTEM micrographs taken from vertically (along the growth axis) and horizontally (lateral view) aligned NRs showed them to have eight facets, {100} and {102}, forming a rhombitruncated hexahedron.[27] Pd_2Sn NR tips were also faceted, as shown in Figure 1b, and three-dimensional (3D) models were obtained using Rhodius software[28] (see animated 3D models in ref 29). The Pd/Sn ratio within Pd−Sn NPs was 2:1, as determined by energy-dispersive X-ray spectroscopy within scanning electron microscopy and confirmed by inductively coupled plasma spectrometry. X-ray diffraction analysis further confirmed Pd−Sn NRs to have a Pd_2Sn orthorhombic crystal structure [Joint Committee on Powder Diffraction Standards (JCPDS) number 00-026-1297; see Figure S2 of the Supporting Information].

The presence of both chloride ions and TOP was critical to produce rod-shaped Pd_2Sn NPs. Moreover, the chlorine and TOP concentrations determined NR size and aspect ratio. Experimental results pointed out that the NR thickness was mainly influenced by the TOP concentration, while the length mainly depended upon the amount of chloride ions (Figure 3).

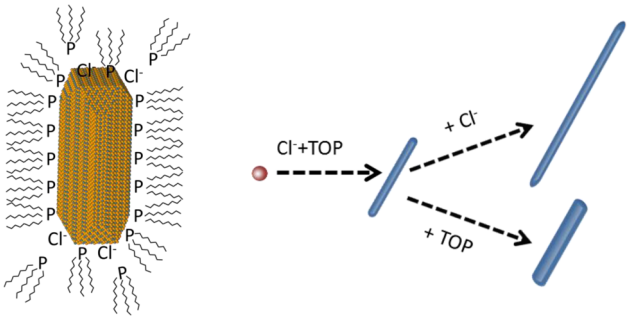

Figure 3. Schematic illustration of the influence of TOP and chloride ions on the shape and size of the Pd_2Sn NRs.

With adjustment of the synthetic conditions (details in section 4 of the Supporting Information), the average NR length could be tuned in the range from 20 to 600 nm and its diameter could be tuned in the range between 6 and 40 nm (Figure 2).

Several theories have been proposed to explain the influence of halide ions on the shape control of Pd,[30] Ag,[31,32] Au,[33−35] and CdSe[36−39] NPs. Halides may modify the reduction potential of the metal ions, passivate specific NP surfaces, or control surface passivation by modulating the concentration of surface ligands.[31−34,40,41] In our system, while OLA played an essential role as coordinating solvent in controlling NP size, TOP and chlorine ions were the key compounds directing Pd_2Sn NP asymmetric growth and determining its aspect ratio. Experimental results evidenced that both TOP and chlorine ions were necessary to produce Pd_2Sn NRs and that they both competed for the passivation of the NR tips (see control experiments in section 5 of the Supporting Information). We believe that a preferential organic ligand desorption from Pd_2Sn

DOI: 10.1021/la504906q
Langmuir XXXX, XXX, XXX−XXX

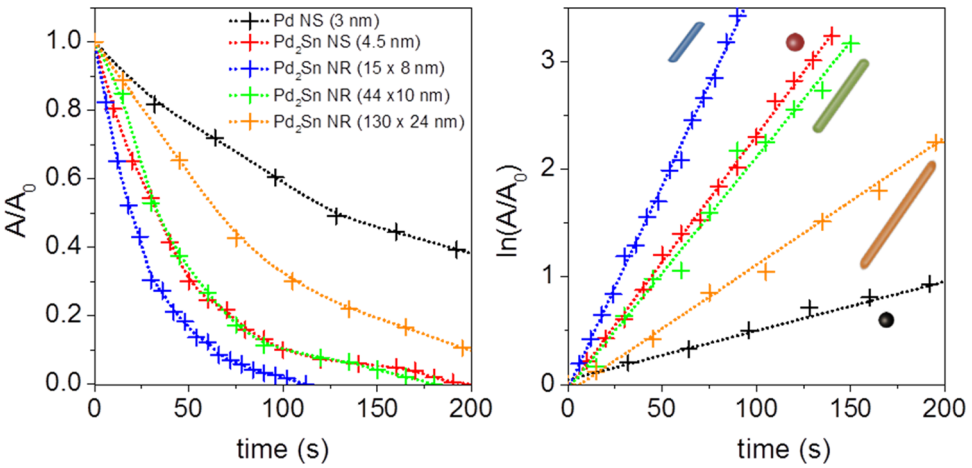

Figure 4. Sodium-borohydride-driven degradation of *p*-nitrophenol over 3.0 nm Pd and 4.3 nm Pd_2Sn spheres, 15 × 8 nm Pd_2Sn NRs, 44 × 10 nm Pd_2Sn NRs, and 130 × 24 nm Pd_2Sn NRs.

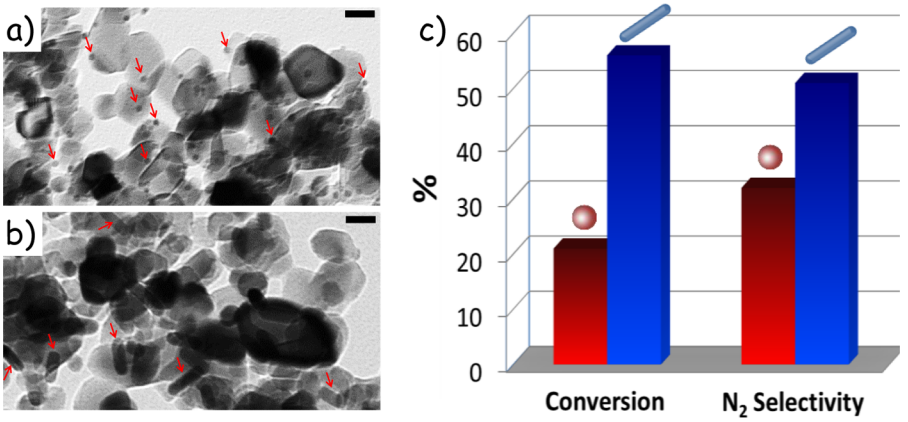

Figure 5. (a and b) TEM images of Pd_2Sn (a) spherical NPs and (b) NRs, supported on TiO_2. Scale bars correspond to 20 nm. (c) Nitrate conversion after 24 h of reaction and N_2 selectivity measured from TiO_2/Pd_2Sn spherical NPs (red) and TiO_2/Pd_2Sn NRs (blue).

NP tip facets directs the growth of asymmetric Pd_2Sn NPs. We hypothesize that, while TOP bonded across the whole NP surface, chlorine ions (harder base than phosphine) induced TOP desorption at the NP tip facets, where a larger density of Sn ions (harder acid than Pd ions) was probably found. From another point of view, rods were formed in the presence of Cl^- because the surface energy differences among the various facets allowed Cl^- to selectively desorb TOP from the (010) facets. These hypotheses are consistent with the larger amounts of TOP providing a more efficient protection of the NR tips, thus resulting in thicker NRs. At the same time, larger amounts of Cl^- displace TOP from the NR tips more efficiently, resulting in longer Pd_2Sn NRs.

An initial evaluation of the functional properties of the new Pd_2Sn NP geometry detailed here was obtained using the reduction of *p*-nitrophenol by sodium borohydride as a model catalytic system.[26] To evaluate and compare NP activity, spherical Pd_2Sn and Pd NPs and Pd_2Sn NRs with three different lengths were rendered soluble in water through ligand exchange with MPA (see the Supporting Information). Figure 4a displays the kinetic of *p*-nitrophenol reduction to *p*-aminophenol in the presence of 3.0 nm Pd (160 m^2/g), 4.3 nm Pd_2Sn spheres (110 m^2/g), 15 × 8 nm Pd_2Sn NRs (50 m^2/g), 44 × 10 nm Pd_2Sn NRs (37 m^2/g), and 130 × 24 nm Pd_2Sn NRs (15 m^2/g).[42] In the presence of an excess of sodium borohydride and sufficient catalysts, the reaction rate could be fitted to a pseudo-first-order reaction, $\ln(A_0/A) = kt$, where k is the apparent rate constant (Figure 4b).[43] Using the exact same total amount (5 mg) and concentration (0.05 mg/mL) of catalytic NPs, 15 × 8 nm Pd_2Sn NRs showed the highest reaction rates, 38 s^{-1} g^{-1} (0.7 s^{-1} m^{-2}). This value was clearly above that measured for spherical Pd_2Sn (23 s^{-1} g^{-1}; 0.2 s^{-1} m^{-2}) and spherical Pd (4.6 s^{-1} g^{-1}; 0.03 s^{-1} m^{-2}) NPs. With normalization for the different surface areas of NRs and spherical NPs, the performance enhancement associated with Pd_2Sn NRs was even more notable, with 3.5- and 28-fold reaction rate increases over spherical Pd_2Sn and Pd NPs, respectively. Such an enhancement of the reaction rates with this particular NR geometry indicates that highly active catalytic sites are located at the NR (100) and/or (102) facets or at the corners between these facets. The reaction rates for longer NRs were 22 s^{-1} g^{-1} (0.6 s^{-1} m^{-2}) for 44 × 10 nm Pd_2Sn NRs and 11 s^{-1} g^{-1} (0.8 s^{-1} m^{-2}) for 130 × 24 nm Pd_2Sn NRs. When the NR length was increased, similar reaction rates per surface area unit were obtained (see Figure S17 of the Supporting Information). However, when the decrease of the surface area is taken into account with the increase of the NR size, lower reaction rates per mass unit were measured when increasing the NR size.

We further compared the activity and selectivity of Pd_2Sn NRs (AR = 1.9) and Pd_2Sn spherical NPs toward water denitration. The removal of nitrate is becoming a major social

DOI: 10.1021/la504906q
Langmuir XXXX, XXX, XXX−XXX

and environmental challenge because nitrate is growing to be one main pollutant of natural aquifers and drinking water produced from groundwater. The catalytic hydrogenation of nitrate to nitrogen is a potential cost-effective and ecological alternative to biological and physicochemical processes of denitrification.[44−46] However, an efficient and selective nitrate hydrogenation requires the synergy between different metals, complicating the catalyst optimization by conventional impregnation methods. Among the different materials tested, Pd-based bimetallic catalysts have shown some of the best conversion rates and selectivities.[25,47,48]

To evaluate Pd_2Sn NP activity toward water denitration, water-soluble spherical Pd_2Sn NPs and Pd_2Sn NRs were supported on Aeroxide TiO_2 P25 with a 5% weight load. Panels a and b of Figure 5 show TEM images of 4.3 ± 0.2 nm Pd_2Sn spherical NPs and 27 ± 2 nm long and 9 ± 1 nm Pd_2Sn NRs, respectively, supported on TiO_2. A constant hydrogen gas flow (150 mL/min) was used as a reducing agent to transform nitrate into nitrogen gas. Experiments were performed in a 350 mL PTFE batch reactor under standard operational conditions (atmospheric pressure and room temperature). Sodium nitrate was used as the nitrate source in ultrapure water. A total of 0.2 g of catalyst was introduced in the 100 ppm nitrate (NO_3^-) solution and remained in suspension by continuously stirring at 500 rpm. Samples were periodically withdrawn to analyze the concentration of NO_3^- and the reduction byproducts, NO_2^- and NH_4^+, by photometry (PC MultiDirect Lovibond) (see the Supporting Information).

Figure 5c shows the percentage of nitrate conversion and the selectivity to N_2 obtained after 24 h of reaction. The catalyst containing 5 wt % Pd_2Sn NRs showed much higher catalytic activity than the spherical NPs; around 3 times higher nitrate conversion was observed. The initial reaction rate for nitrate removal was 21.7 mg h^{-1} g^{-1} (0.5 mg h^{-1} m^{-2}) of metal and 7.4 mg h^{-1} g^{-1} (0.06 mg h^{-1} m^{-2}) of metal for NRs and spherical NPs, respectively. The selectivity to nitrogen for NRs was higher (51%) than that for spherical NPs (32%). Furthermore, the NH_4^+ formation (5% of selectivity) was lower than other reported Pd−Sn catalysts, e.g., the catalyst reported by Palomares et al.[49] (around 40% of selectivity to NH_4^+). The hydrogen chemisorption technique (see the Supporting Information) was applied on both catalysts to determine palladium dispersion. The 5% Pd_2Sn NRs exhibited a dispersion of 0.37%, while the 5% Pd_2Sn spherical NPs showed a lower dispersion (0.16%). These very low values of metal dispersion indicate that the formation of the PdSn alloy inhibits the hydrogen chemisorption, as reported by other authors.[50,51] Consequently, the alloy formation could be responsible for the lower selectivity to NH_4^+, reducing the over-hydrogenation reaction.

CONCLUSION

In summary, we detailed a procedure to produce Pd_2Sn NRs with controlled size and aspect ratio. The growth mechanism was based on the selective desorption of TOP by chlorine ions. Pd_2Sn NRs showed higher catalytic performance than smaller spherical NPs toward reduction of *p*-nitrophenol by sodium borohydride and water denitration. Enhanced catalytic properties must be associated with the more active surface facets of Pd_2Sn NRs. A systematic optimization of the catalyst, which should probably involve the decrease of the NR dimensions, is now required to maximize its catalytic activity and selectivity in several potential applications of this material.

ASSOCIATED CONTENT

Supporting Information

TEM micrograph of spherical Pd NPs, geometric and crystal structure characterization, control experiments, and details of the *p*-nitrophenol reduction, EOR, and water denitration experiments. This material is available free of charge via the Internet at http://pubs.acs.org.

AUTHOR INFORMATION

Corresponding Author

*E-mail: acabot@irec.cat.

Notes

The authors declare no competing financial interest.

ACKNOWLEDGMENTS

This work was supported by the European Regional Development Funds, Generalitat de Catalunya 2014SGR1638, and Spanish MINECO under Contracts ENE2013-46624-C4-3-R and CSD2009-00050. ZhiShan Luo thanks the China Scholarship Council (CSC 201206740024) for scholarship support. Maria Ibáñez thanks AGAUR for her Beatriu i Pinós (2013 BP-A 00344) postdoctoral grant. Aziz Genç acknowledges the scholarship from the Ministry of National Education of Turkey.

REFERENCES

(1) Herranz, T.; Ibáñez, M.; Gómez de la Fuente, J. L.; Pérez-Alonso, F. J.; Peña, M. A.; Cabot, A.; Rojas, S. *In situ* study of ethanol electrooxidation on monodispersed Pt_3Sn nanoparticles. *ChemElectroChem* **2014**, *1*, 885−895.

(2) Flox, C.; Rubio-Garcia, J.; Nafria, R.; Zamani, R.; Skoumal, M.; Andreu, T.; Arbiol, J.; Cabot, A.; Morante, J. R. Active nano-$CuPt_3$ electrocatalyst supported on graphene for enhancing reactions at the cathode in all-vanadium redox flow batteries. *Carbon* **2012**, *50*, 2372−2374.

(3) Porter, N. S.; Wu, H.; Quan, Z.; Fang, J. Shape-control and electrocatalytic activity-enhancement of Pt-based bimetallic nanocrystals. *Acc. Chem. Res.* **2013**, *46*, 1867−1877.

(4) Shao, M.; Liu, P.; Zhang, J.; Adzic, R. Origin of enhanced activity in palladium alloy electrocatalysts for oxygen reduction reaction. *J. Phys. Chem. B* **2007**, *111*, 6772−6775.

(5) Yang, X.; Hu, J.; Fu, J.; Wu, R.; Koel, B. E. Role of surface iron in enhanced activity for the oxygen reduction reaction on a $Pd_3Fe(111)$ single-crystal alloy. *Angew. Chem., Int. Ed.* **2011**, *50*, 10182−10185.

(6) Shao, M.-H.; Sasaki, K.; Adzic, R. R. Pd−Fe nanoparticles as electrocatalysts for oxygen reduction. *J. Am. Chem. Soc.* **2006**, *128*, 3526−3527.

(7) Kim, S.-W.; Kim, M.; Lee, W. Y.; Hyeon, T. Fabrication of hollow palladium spheres and their successful application to the recyclable heterogeneous catalyst for Suzuki coupling reactions. *J. Am. Chem. Soc.* **2002**, *124*, 7642−7643.

(8) Son, S. U.; Jang, Y.; Park, J.; Na, H. B.; Park, H. M.; Yun, H. J.; Lee, J.; Hyeon, T. Designed synthesis of atom-economical Pd/Ni bimetallic nanoparticle-based catalysts for Sonogashira coupling reactions. *J. Am. Chem. Soc.* **2004**, *126*, 5026−5027.

(9) Yin; Liebscher, J. Carbon−carbon coupling reactions catalyzed by heterogeneous palladium catalysts. *Chem. Rev.* **2006**, *107*, 133−173.

(10) Xia, Y.; Xiong, Y.; Lim, B.; Skrabalak, S. E. Shape-controlled synthesis of metal nanocrystals: Simple chemistry meets complex physics? *Angew. Chem., Int. Ed.* **2009**, *48*, 60−103.

(11) Kariuki, N. N.; Wang, X.; Mawdsley, J. R.; Ferrandon, M. S.; Niyogi, S. G.; Vaughey, J. T.; Myers, D. J. Colloidal synthesis and characterization of carbon-supported Pd−Cu nanoparticle oxygen reduction electrocatalysts. *Chem. Mater.* **2010**, *22*, 4144−4152.

(12) Zhang, L.; Hou, F.; Tan, Y. Shape-tailoring of CuPd nanocrystals for enhancement of electro-catalytic activity in oxygen reduction reaction. *Chem. Commun.* **2012**, *48*, 7152−7154.

DOI: 10.1021/la504906q
Langmuir XXXX, XXX, XXX−XXX

(13) Tang, W.; Zhang, L.; Henkelman, G. Catalytic activity of Pd/Cu random alloy nanoparticles for oxygen reduction. *J. Phys. Chem. Lett.* **2011**, *2*, 1328−1331.
(14) Jin, M.; Zhang, H.; Wang, J.; Zhong, X.; Lu, N.; Li, Z.; Xie, Z.; Kim, M. J.; Xia, Y. Copper can still be epitaxially deposited on palladium nanocrystals to generate core−shell nanocubes despite their large lattice mismatch. *ACS Nano* **2012**, *6*, 2566−2573.
(15) Gao, Q.; Ju, Y.-M.; An, D.; Gao, M.-R.; Cui, C.-H.; Liu, J.-W.; Cong, H.-P.; Yu, S.-H. Shape-controlled synthesis of monodisperse PdCu nanocubes and their electrocatalytic properties. *ChemSusChem* **2013**, *6*, 1878−1882.
(16) Mazumder, V.; Chi, M.; Mankin, M. N.; Liu, Y.; Metin, Ö.; Sun, D.; More, K. L.; Sun, S. A facile synthesis of MPd (M = Co, Cu) nanoparticles and their catalysis for formic acid oxidation. *Nano Lett.* **2012**, *12*, 1102−1106.
(17) Hokenek, S.; Bennett, C.; Kuhn, J. N. Synthesis of Ni−Pd nanocubes and nanorods with high selectivity through a modified polyol process. *J. Cryst. Growth* **2013**, *374*, 18−22.
(18) Rupprechter, G.; Weilach, C. Mind the gap! Spectroscopy of catalytically active phases. *Nano Today* **2007**, *2*, 20−29.
(19) Long, R.; Mao, K.; Ye, X.; Yan, W.; Huang, Y.; Wang, J.; Fu, Y.; Wang, X.; Wu, X.; Xie, Y.; Xiong, Y. Surface facet of palladium nanocrystals: A key parameter to the activation of molecular oxygen for organic catalysis and cancer treatment. *J. Am. Chem. Soc.* **2013**, *135*, 3200−3207.
(20) Narayanan, R.; El-Sayed, M. A. Effect of colloidal nanocatalysis on the metallic nanoparticle shape: The Suzuki reaction. *Langmuir* **2005**, *21*, 2027−2033.
(21) Heemeier, M.; Carlsson, A. F.; Naschitzki, M.; Schmal, M.; Bäumer, M.; Freund, H.-J. Preparation and characterization of a model bimetallic catalyst: Co−Pd nanoparticles supported on Al_2O_3. *Angew. Chem., Int. Ed.* **2002**, *41*, 4073−4076.
(22) Du, W.; Mackenzie, K. E.; Milano, D. F.; Deskins, N. A.; Su, D.; Teng, X. Palladium−tin alloyed catalysts for the ethanol oxidation reaction in an alkaline medium. *ACS Catal.* **2012**, *2*, 287−297.
(23) Jou, L.-H.; Chang, J.-K.; Whanga, T.-J.; Sun, I.-W. Electrodeposition of palladium−tin alloys from 1-ethyl-3-methylimidazolium chloride−tetrafluoroborate ionic liquid for ethanol electro-oxidation. *J. Electrochem. Soc.* **2010**, *157*, D443−D449.
(24) Barbosa, D. P.; Tchiéta, P.; Rangel, M. d. C.; Epron, F. The use of a cation exchange resin for palladium−tin and palladium−indium catalysts for nitrate removal in water. *J. Mol. Catal. A: Chem.* **2013**, *366*, 294−302.
(25) Garron, A.; Lázár, K.; Epron, F. Effect of the support on tin distribution in Pd−Sn/Al_2O_3 and Pd−Sn/SiO_2 catalysts for application in water denitration. *Appl. Catal., B* **2005**, *59*, 57−69.
(26) Hayakawa, K.; Yoshimura, T.; Esumi, K. Preparation of gold−dendrimer nanocomposites by laser irradiation and their catalytic reduction of 4-nitrophenol. *Langmuir* **2003**, *19*, 5517−5521.
(27) Barnard, A. S.; Osawa, E. The impact of structural polydispersivity on the surface electrostatic potential of nanodiamond. *Nanoscale* **2014**, *6*, 1188−1194.
(28) Bernal, S.; Botana, F. J.; Calvino, J. J.; López-Cartes, C.; Pérez-Omil, J. A.; Rodríguez-Izquierdo, J. M. The interpretation of HREM images of supported metal catalysts using image simulation: Profile view images. *Ultramicroscopy* **1998**, *72*, 135−164.
(29) www.icmab.es/gaen/research/240.
(30) Zhang, H.; Jin, M.; Xiong, Y.; Lim, B.; Xia, Y. Shape-controlled synthesis of Pd nanocrystals and their catalytic applications. *Acc. Chem. Res.* **2012**, *46*, 1783−1794.
(31) Wiley, B.; Herricks, T.; Sun, Y.; Xia, Y. Polyol synthesis of silver nanoparticles: Use of chloride and oxygen to promote the formation of single-crystal, truncated cubes and tetrahedrons. *Nano Lett.* **2004**, *4*, 1733−1739.
(32) Cathcart, N.; Frank, A. J.; Kitaev, V. Silver nanoparticles with planar twinned defects: Effect of halides for precise tuning of plasmon resonance maxima from 400 to >900 nm. *Chem. Commun.* **2009**, 7170−7172.
(33) Millstone, J. E.; Wei, W.; Jones, M. R.; Yoo, H.; Mirkin, C. A. Iodide ions control seed-mediated growth of anisotropic gold nanoparticles. *Nano Lett.* **2008**, *8*, 2526−2529.
(34) DuChene, J. S.; Niu, W.; Abendroth, J. M.; Sun, Q.; Zhao, W.; Huo, F.; Wei, W. D. Halide anions as shape-directing agents for obtaining high-quality anisotropic gold nanostructures. *Chem. Mater.* **2012**, *25*, 1392−1399.
(35) Gómez-Graña, S.; Goris, B.; Altantzis, T.; Fernández-López, C.; Carbó-Argibay, E.; Guerrero-Martínez, A.; Almora-Barrios, N.; López, N.; Pastoriza-Santos, I.; Pérez-Juste, J.; Bals, S.; Van Tendeloo, G.; Liz-Marzán, L. M. Au@Ag nanoparticles: Halides stabilize {100} facets. *J. Phys. Chem. Lett.* **2013**, *4*, 2209−2216.
(36) Lim, S. J.; Kim, W.; Jung, S.; Seo, J.; Shin, S. K. Anisotropic etching of semiconductor nanocrystals. *Chem. Mater.* **2011**, *23*, 5029−5036.
(37) Iacono, F.; Palencia, C.; de la Cueva, L.; Meyns, M.; Terracciano, L.; Vollmer, A.; de la Mata, M. J.; Klinke, C.; Gallego, J. M.; Juarez, B. H.; Otero, R. Interfacing quantum dots and graphitic surfaces with chlorine atomic ligands. *ACS Nano* **2013**, *7*, 2559−2565.
(38) Meyns, M.; Bastus, N. G.; Cai, Y.; Kornowski, A.; Juarez, B. H.; Weller, H.; Klinke, C. Growth and reductive transformation of a gold shell around pyramidal cadmium selenide nanocrystals. *J. Mater. Chem.* **2010**, *20*, 10602−10605.
(39) Palencia, C.; Lauwaet, K.; de la Cueva, L.; Acebron, M.; Conde, J. J.; Meyns, M.; Klinke, C.; Gallego, J. M.; Otero, R.; Juarez, B. H. Cl-Capped CdSe nanocrystals via *in situ* generation of chloride anions. *Nanoscale* **2014**, *6*, 6812−6818.
(40) Kim, M. R.; Miszta, K.; Povia, M.; Brescia, R.; Christodoulou, S.; Prato, M.; Marras, S.; Manna, L. Influence of chloride ions on the synthesis of colloidal branched CdSe/CdS nanocrystals by seeded growth. *ACS Nano* **2012**, *6*, 11088−11096.
(41) Lohse, S. E.; Burrows, N. D.; Scarabelli, L.; Liz-Marzán, L. M.; Murphy, C. J. Anisotropic noble metal nanocrystal growth: The role of halides. *Chem. Mater.* **2013**, *26*, 34−43.
(42) Zeng, J.; Zhang, Q.; Chen, J.; Xia, Y. A comparison study of the catalytic properties of Au-based nanocages, nanoboxes, and nanoparticles. *Nano Lett.* **2009**, *10*, 30−35.
(43) Lee, J.; Park, J. C.; Song, H. A nanoreactor framework of a Au@SiO_2 yolk/shell structure for catalytic reduction of *p*-nitrophenol. *Adv. Mater.* **2008**, *20*, 1523−1528.
(44) Aristizábal, A.; Contreras, S.; Divins, N. J.; Llorca, J.; Medina, F. Pt−Ag/activated carbon catalysts for water denitration in a continuous reactor: Incidence of the metal loading, Pt/Ag atomic ratio and Pt metal precursor. *Appl. Catal., B* **2012**, *127*, 351−362.
(45) Aristizábal, A.; Contreras, S.; Divins, N. J.; Llorca, J.; Medina, F. Effect of impregnation protocol in the metallic sites of Pt−Ag/activated carbon catalysts for water denitration. *Appl. Surf. Sci.* **2014**, *298*, 75−89.
(46) Prüsse, U.; Hähnlein, M.; Daum, J.; Vorlop, K.-D. Improving the catalytic nitrate reduction. *Catal. Today* **2000**, *55*, 79−90.
(47) Dodouche, I.; Barbosa, D. P.; Rangel, M. d. C.; Epron, F. Palladium−tin catalysts on conducting polymers for nitrate removal. *Appl. Catal., B* **2009**, *93*, 50−55.
(48) Lemaignen, L.; Tong, C.; Begon, V.; Burch, R.; Chadwick, D. Catalytic denitrification of water with palladium-based catalysts supported on activated carbons. *Catal. Today* **2002**, *75*, 43−48.
(49) Palomares, A. E.; Franch, C.; Corma, A. A study of different supports for the catalytic reduction of nitrates from natural water with a continuous reactor. *Catal. Today* **2011**, *172*, 90−94.
(50) Tanielyan, S. K.; Augustine, R. L. Acetoxylation of toluene catalyzed by supported Pd−Sn catalysts. *J. Mol. Catal.* **1994**, *87*, 311−328.
(51) Rochefort, A.; Andzelm, J.; Russo, N.; Salahub, D. R. Chemisorption and diffusion of atomic hydrogen in and on cluster models of palladium, rhodium and bimetallic palladium tin, rhodium tin, and rhodium zinc catalysts. *J. Am. Chem. Soc.* **1990**, *112*, 8239−8247.

DOI: 10.1021/la504906q
Langmuir XXXX, XXX, XXX−XXX